JACS
JOURNAL OF THE AMERICAN CHEMICAL SOCIETY

ARTICLE

pubs.acs.org/JACS

Degradable Self-Assembling Dendrons for Gene Delivery: Experimental and Theoretical Insights into the Barriers to Cellular Uptake

Anna Barnard,[†] Paola Posocco,[‡] Sabrina Pricl,[‡] Marcelo Calderon,[§] Rainer Haag,[§] Mark E. Hwang,[∥] Victor W. T. Shum,[∥] Daniel W. Pack,[∥] and David K. Smith*[,†]

[†]Department of Chemistry, University of York, Heslington, York, YO10 5DD, U.K.

[‡]Molecular Simulation Engineering (MOSE) Laboratory, Department of Industrial Engineering and Information Technology (DI3), University of Trieste, 34127 Trieste, Italy

[§]Institut für Chemie und Biochemie, Freie Universität Berlin, Takustrasse 3, D-14195 Berlin, Germany

[∥]Department of Chemical and Biomolecular Engineering, University of Illinois at Urbana−Champaign, Urbana, Illinois 61801, United States

Supporting Information

ABSTRACT: This paper uses a combined experimental and theoretical approach to gain unique insight into gene delivery. We report the synthesis and investigation of a new family of second-generation dendrons with four triamine surface ligands capable of binding to DNA, degradable aliphatic-ester dendritic scaffolds, and hydrophobic units at their focal points. Dendron self-assembly significantly enhances DNA binding as monitored by a range of experimental methods and confirmed by multiscale modeling. Cellular uptake studies indicate that some of these dendrons are highly effective at transporting DNA into cells (ca. 10 times better than poly(ethyleneimine), PEI). However, levels of transgene expression are relatively low (ca. 10% of PEI). This indicates that these dendrons cannot navigate all of the intracellular barriers to gene delivery. The addition of chloroquine indicates that endosomal escape is not the limiting factor in this case, and it is shown, both experimentally and theoretically, that gene delivery can be correlated with the ability of the dendron assemblies to release DNA. Mass spectrometric assays demonstrate that the dendrons, as intended, do degrade under biologically relevant conditions over a period of hours. Multiscale modeling of degraded dendron structures suggests that complete dendron degradation would be required for DNA release. Importantly, in the presence of the lower pH associated with endosomes, or when bound to DNA, complete degradation of these dendrons becomes ineffective on the transfection time scale—we propose this explains the poor transfection performance of these dendrons. As such, this paper demonstrates that taking this kind of multidisciplinary approach can yield a fundamental insight into the way in which dendrons can navigate barriers to cellular uptake. Lessons learned from this work will inform future dendron design for enhanced gene delivery.

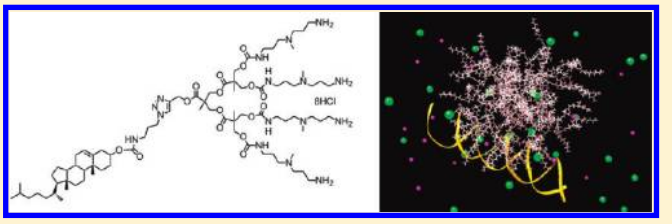

INTRODUCTION

Dendrons have been suggested as appropriate nanoscale carrier molecules for the delivery of bioactive materials into cells.[1] These branched, well-defined, wedge-like molecular structures are highly tunable using simple organic synthesis—for example, it is possible to modify the functional groups present at the focal point, those within the branching, and also those displayed on the dendritic surface. This means that a huge variety of potentially bioactive dendrons can be accessed with relative ease.[1] Each part of the dendron can play a distinctive role in controlling the biological behavior. Choice of an appropriate hydrophobic group at the dendron focal point can give rise to controlled self-assembly into larger nanoscale aggregates,[2] with the relative size of the hydrophobic and hydrophilic groups controlling the architecture of the resulting self-assembled structure.[3] The multiple surface groups of a dendron constitute an optimum multivalent array for displaying bioactive ligands—such arrays significantly enhance the binding affinity for key biological targets as a consequence of the entropic benefits of ligand organization.[4] It is also possible to make the dendritic branched scaffold degradable, such that over time, or in the presence of specific biological triggers, it breaks down in a controllable and predictable way into smaller subunits.[5] This can enhance the biocompatibility of the dendron, lower its toxicity, and limit its persistence in cells. Dendron degradation also disassembles the multivalent array and therefore acts as an effective way of "switching off" the multivalent binding effect, significantly decreasing the affinity of the system for the biological target.[6,7]

Received: July 28, 2011
Published: October 31, 2011

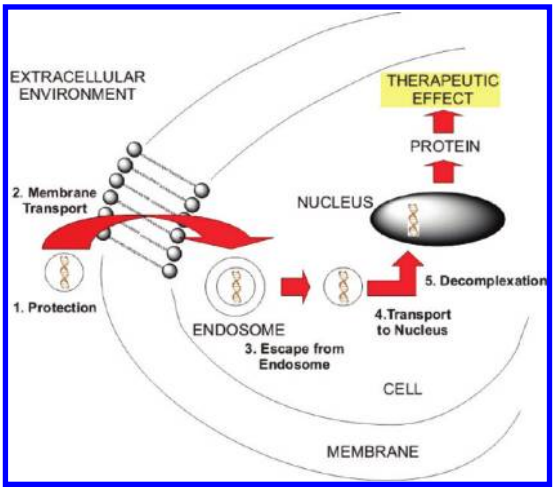

Figure 1. Schematic of gene delivery process, highlighting the barriers which have to be overcome by effective vectors.

Dendrons (and spherical dendrimers) have been of particular interest as a consequence of their ability to deliver genetic material into cells.[8] Since the pioneering work from the groups of Tomalia[9] and Szoka[10] using poly(amidoamine) spherical dendrimers, a wide range of different dendritic architectures have been explored for their gene delivery potential. In most cases, large polycationic dendrimers based on polyamines such as dendritic poly-L-lysine have been employed.[11] Such systems can be considered to belong to the cationic polymer class of gene delivery vehicle.[12] Although such systems can perform highly effective gene delivery, they also exhibit problematic toxicity profiles[13] and can cause difficulties as a consequence of their persistence in cells after gene delivery has taken place.[14] An alternative approach has therefore used dendron architectures in which a hydrophobic group at the focal point encourages self-assembly of the dendrons into a larger "pseudodendrimer". Such systems, reported by the groups of Diederich,[15] Florence,[16] and Hammond,[17] are also capable of binding DNA and delivering it into cells. Dendrons of this type are somewhat closer in nature to the cationic lipid class of gene delivery vehicle.[18]

For effective gene delivery into cells, it is necessary to overcome a number of extra- and intracellular barriers.[19] To achieve effective gene delivery, a synthetic vector must: (1) complex and protect the DNA in the extracellular environment, (2) enable transit of the cell membrane—usually via endosomal uptake mechanisms, (3) allow escape from the endosomal vesicles within the cell after uptake, (4) enable transit to and entry into the cell nucleus, (5) release the DNA so that it can be effectively translated into the desired protein, and (6) (not shown) degrade such that the vector does not persist and cause problems within the cell once delivery has taken place (Figure 1).[14] Gene delivery is therefore a challenging target, and as of yet, although synthetic vectors are used commercially for in vitro applications, there has only been limited success using synthetic gene delivery vehicles for in vivo work.[20]

Since 2005, we have been reporting on a family of dendrons designed to show ultrahigh-affinity DNA binding[21] and explored their ability to deliver genetic material into cells.[22] By modifying the dendrons with different hydrophobic groups at the focal point, we have demonstrated that self-assembly of the dendrons takes place, with their gene delivery ability correlating with the nanoscale architecture into which the dendrons assemble.[3,23] This approach has enabled us to develop a detailed understanding of structure—activity relationships and multivalency effects in DNA binding and gene delivery.[24] In recent years, to improve biocompatibility, the attention of Kostiainen and ourselves has turned to biodegradable dendron frameworks,[6,7] and in 2009, we reported a simple system based on Fréchet-type aliphatic ester dendrons[25] modified with spermine surface groups which exhibited multivalent binding and degraded such that DNA binding became disfavored in vitro.[7]

In this paper, we modified the focal point of these dendrons, replacing the Z-protecting group with hydrophobic units (Figure 2), promoting dendron self-assembly. We have also changed the surface groups, replacing them with a triamine, which we have previously reported lowers the toxicity of the dendron constructs.[24b] We have then experimentally measured the effect of these modifications on DNA binding and cellular gene delivery as well as monitored the degradation of the dendrons using an in vitro mass spectrometric assay. We have then modeled the behavior of both the intact and the degraded dendrons using a mesoscale approach and monitored their ability to self-assemble and bind DNA. Using this powerful combination of experimental and theoretical approaches, we gain a unique insight into the gene delivery process and a detailed understanding of the way in which these systems negotiate each of the barriers to gene delivery.

RESULTS AND DISCUSSION

Dendron Synthesis and Characterization. The synthesis and characterization data for all compounds are provided in the Supporting Information (SI). In summary, second-generation dendrons with amine groups on the surface and an alkyne functional group at the focal point were synthesized using a combination of the methodology previously reported by Fréchet,[25] Sharpless,[26] and ourselves.[27] We then employed "click' chemistry methods to conjugate azide-functionalized hydrophobic units to the focal point of the alkyne-modified dendron (see SI for full synthetic schemes). Appropriate azides were prepared according to the methods outlined in the SI. After coupling of the azides to the alkyne group, compound purification yielded the modified dendrons with hydrophobic groups connected at the focal point via a triazole linkage. The Boc protecting groups were finally removed from the amine surface ligands using HCl gas. This gave rise to the target compounds, **Chol-G2**, **Chol$_2$-G2**, **C$_{12}$-G2**, **C$_{16}$-G2**, and **C$_{22}$-G2** (Figure 2). As a control, we also synthesized **Z-G2** (Figure 2) in which a simple benzyl ester protecting group is present at the focal point of the dendron. All intermediate compounds were fully characterized, and all target compounds were synthesized in good overall yields and fully characterized (see SI).

Self-Assembly of Dendrons. Initially, we monitored whether the dendrons aggregated in aqueous solution, using solubilization experiments with the hydrophobic dye Nile Red.[28] If self-assembled architectures are present, Nile Red is solubilized into the hydrophobic domain of the aggregates. Varying the concentration of the self-assembling peptide will then lead to increasing levels of dye solubilization. Plotting the fluorescence emission intensity of Nile Red at 635 nm versus $\log_{10}$[dendron] allows the determination of critical micelle concentrations (CMCs) (see SI for data). Table 1 reports the CMC values for the six dendrons investigated in this paper. As can be seen from the data, the functional group at the dendron focal point has a profound effect on the dendron aggregation process. Control compound **Z-G2**

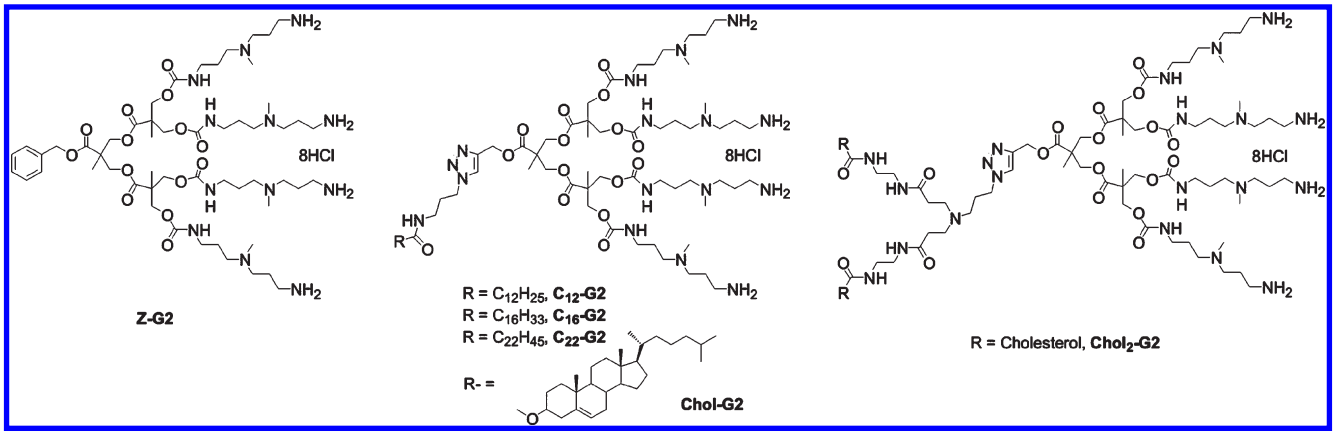

Figure 2. Dendrons investigated in this paper.

Table 1. Self-Assembly Data for Dendrons Investigated in This Paper

compound	CMC (μM)[a]	zeta (mV)[b]	diameter (nm)[b]
Z-G2	N/A	+34.1 ± 1.8	does not fit DLS model
C_{12}-G2	208 ± 56	+42.6 ± 2.0	does not fit DLS model
C_{16}-G2	37 ± 6	+45.0 ± 1.9	5.93 ± 0.65
C_{22}-G2	2.0 ± 0.1	+56.1 ± 3.2	6.96 ± 0.18
Chol-G2	4.9 ± 0.6	+56.3 ± 4.4	7.55 ± 0.04
$Chol_2$-G2	4.9 ± 0.6	+55.4 ± 2.2	15.04 ± 0.65

[a] The CMC is the critical micelle concentration as determined from the Nile Red assay. [b] Zeta potential and average diameter assessed by zeta sizing and intensity distribution in DLS measurements, respectively.

Table 2. Modeling of Dendron Self-Assembly by Mesoscale Methods

compound	D_m[a]	R_c[b]	N_{agg}[c]	σ_m[d]	ΔG_{mic}[e]	CMC[f]
C_{12}-G2	2.9 ± 0.1	0.8	6	1.77	−63.6	2.7
C_{16}-G2	3.1 ± 0.1	0.9	7	1.89	−75.7	0.23
C_{22}-G2	3.3 ± 0.2	1.0	9	2.09	−92.3	0.080
Chol-G2	3.9 ± 0.2	1.1	16	2.68	−96.4	0.035
$Chol_2$-G2	5.1 ± 0.1	1.5	22	2.15	−99.6	0.018

[a] D_m (diameter of the micelle in nm). [b] R_c (radius of the micellar core in nm). [c] N_{agg} (aggregation number, i.e., the number of dendrons in a micelle). [d] σ_m (surface charge density of the micelle in e nm^{-2}). [e] ΔG_{mic} (predicted free energy of micellization in kJ mol^{-1}). [f] CMC (predicted critical micelle concentration in μM).

did not show any evidence of aggregation under the conditions assayed (up to 1 mM). For the alkyl chain modified dendrons, there is an inverse relationship between the length of the hydrophobic chain and the CMC value. As the hydrophobic chain increases in length from **C_{12}-G2** to **C_{16}-G2** to **C_{22}-G2**, the CMC value drops from 208 to 2 μM, a consequence of more effective packing of the longer hydrophobic chains resulting in better self-assembly. Both cholesterol-functionalized dendrons exhibited similar CMC values of ca. 5 μM. Clearly, cholesterol is quite effective in encouraging the self-organization of these dendrons.

The aggregates were also investigated by zeta sizing methods to estimate the sizes and surface charges of the self-assembled "pseudodendrimers" being formed by these compounds, with the diameters reported being based on the volume contribution (Table 1). As can be seen, the data were in general agreement with the Nile Red assay, in showing that the dendrons with the most extensive hydrophobic functionalization at the focal point are best able to self-assemble into structured aggregates. Specifically, compounds **Z-G2** and **C_{12}-G2** only fitted poorly to the dynamic light scattering (DLS) model, exhibiting relatively low zeta potentials indicative of low positive charge densities. This is consistent with the results of the Nile Red assay which indicated that these compounds have low self-assembly potential. Conversely, compounds **Chol-G2**, **$Chol_2$-G2**, and **C_{22}-G2**, all of which have significant hydrophobic groups attached at the focal point and formed aggregates with CMCs < 10 μM according to the Nile Red assay, appeared to form well-defined aggregates via the zeta sizing method. Furthermore, those systems with the greatest potential to self-assemble achieved the highest surface charge potential, of ca. +56 mV. This would seem to indicate that favorable energetic terms associated with the self-assembly of the hydrophobic functional groups are able to drive the close-packing of positively charged groups on the surfaces of the nanoscale assembled architectures. Interestingly, as the size of the hydrophobic unit increases, so does the apparent diameter of the micellar aggregates, from ca. 5.9 nm for **C_{16}-G2** to 7.0 nm for **C_{22}-G2** and 7.5 nm for **Chol-G2**. Intriguingly, the assemblies formed by **Chol-G2** were significantly different from those formed by **$Chol_2$-G2**, and although they exhibited roughly the same zeta potential values, the diameters of the observed complexes were ca. 7.5 and 15.0 nm, respectively.

We employed mesoscale modeling methods to better understand the eventual self-assembly of all modified dendrons. Mesoscale methods are ideal for modeling nanoscale self-assembly processes, as they are able to cope with spatial inhomogeneities over the nanometer length scale, as well as variable phenomena over longer time scales (up to milliseconds). We chose to use dissipative particle dynamics (DPD) to model these self-assemblies.[29] In DPD, a group of atoms is coarse-grained into a bead, thereby substantially reducing the number of particles to be simulated. Further, rather than interact through Lennard-Jones forces, the beads feel a simple soft pairwise conservative potential which embodies the essential chemistry of the system. This modeling was carried out in a biorelevant aqueous solvent environment, in the presence of NaCl (150 mM).

As indicated by the data in Table 2, with the exception of **Z-G2**, all the remaining dendrons self-assembled into nanoscale

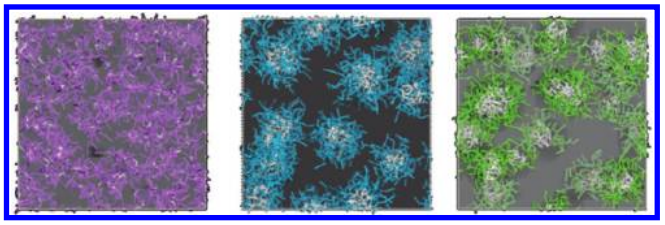

Figure 3. Mesoscale modeling of the hydrophobically modified **Z-G2** (left), **Chol-G2** (center), and **C_{22}-G2** (right). The white sticks represent the hydrophobic units. Different colored sticks (purple, light blue, and green) are adopted to represent the various hydrophilic regions. A transparent gray field is used to portray water.

objects under mesoscale modeling conditions. Israelachvili reported that the packing parameter, *P* (an effective ratio of hydrophobic/hydrophilic size), could be used to predict the shape of nanoscale aggregates for ionic amphiphiles.[30] Adopting the same concept in the present case, for all modified dendrons, this value is <0.33 and would lead us to predict that all dendrons but **Z-G2** would self-assemble into spherical micelles, as observed in the modeling (Figure 3 and Figure S8.3, SI).

Importantly, the predicted CMC values follow the correct, increasing trend as the hydrophobic character of the dendron substituents decreases. For example, on going from **C_{22}-G2** to **C_{16}-G2** to **C_{12}-G2**, as the hydrophobic chain becomes shorter, the CMC increases. This is in general agreement with the results of the Nile Red assay. Furthermore, the micellar surface charge density (σ_m) increases as the hydrophobic chain lengthens and becomes better able to pack—in agreement with the measurements of zeta potentials (Table 1). Modeling indicates that **$Chol_2$-G2** should have a lower CMC than **Chol-G2**, although this was not observed experimentally—but it is well-known that the use of dyes such as Nile Red can lead to perturbations in the apparent aggregation. Notably, even if these CMC values estimated in silico are taken with due caution, they are below the experimental concentrations employed in the transfection experiments, and the presence of micelles as nanovectors is therefore supported by the modeling.

It was predicted from modeling (Table 2) that the average micellar diameter increases as the hydrocarbon content of the hydrophobic chain increases—in agreement with the trends found in the experimental study (Table 1). Interestingly, the different architectures of the hydrophobic portion ultimately result in differently sized micelles and/or a different number of dendrons per micelle (the aggregation number N_{agg}) and, hence, a different micellar surface charge density σ_m. Comparing **Chol-G2** and **$Chol_2$-G2** with the other modified dendrons, we see that these compounds assemble into micelles of bigger diameters than the other counterparts. This is likely due to the highly hydrophobic nature and flat, rigid cholesterol moieties leading to highly effective packing within the micellar interior. Also, comparing the two cholesterol-bearing molecules, modeling predicts the formation of larger micelles for **$Chol_2$-G2** than **Chol-G2**. These larger aggregates are a consequence of the fact that a larger number of **$Chol_2$-G2** are incorporated into each micelle compared with **Chol-G2** (22 molecules per micelle rather than 16) and due to the two cholesterol units at the focal point providing a more favorable free energy of micellization (by ca. 3 kJ mol^{-1}). This modeling is in general agreement with the results of zeta sizing, which indicated that **$Chol_2$-G2** did indeed form the largest aggregates, followed by **Chol-G2**, **C_{22}-G2**, and **C_{16}-G2**, respectively.

Table 3. DNA Binding Data for Dendrons Investigated in This Paper

compound	CE_{50} (EthBr assay)[a]	N:P (gel assay)[b]
Z-G2	N/A	4.61
C_{12}-G2	N/A	2.38
C_{16}-G2	1.42 ± 0.80	2.30
C_{22}-G2	0.84 ± 0.34	2.20
Chol-G2	0.66 ± 0.13	2.09
$Chol_2$-G2	0.57 ± 0.03	1.82

[a] The CE_{50} value is the charge excess required for 50% displacement of ethidium bromide in the fluorescence displacement assay. [b] The N:P value is the charge excess required for retention of 1 μg of plasmid DNA in the well in the gel electrophoresis assay.

Although it is predicted that the micelles formed by **Chol-G2** and **$Chol_2$-G2** are somewhat different in terms of their dimensions, it is noteworthy that the surface charges (σ_m) of the two self-assembled dendron micelles are fairly comparable, with **Chol-G2** having a slightly higher surface charge. Once again, this is in good agreement with the results of zeta sizing, which indicated the **Chol-G2** and **$Chol_2$-G2** aggregates had surface charges of +56.3 and +55.4 mV, respectively. Consequently, the combined experimental and theoretical approach convinced us that we had a good understanding of the dendron self-assembly process.

DNA Binding Studies. We then went on to assay the ability of these dendrons to bind DNA. Initially we bound calf thymus DNA using the standard ethidium bromide (EthBr) displacement fluorescence spectroscopy assay which we have employed in our previous research.[7,21,31] This method uses competition between the DNA binder and EthBr to assess the concentration at which the DNA binder becomes effective. This can be expressed as the concentration of DNA binder required for half of the EthBr to be displaced from binding to DNA. This concentration can usefully be expressed as a charge excess (CE_{50}) value. To calculate this CE_{50} value, it is assumed that each amine in the DNA binder is protonated, and each phosphate in the DNA is deprotonated. As such, the CE_{50} value is equivalent to a N:P ratio. Lower CE_{50} values represent more effective binding, as a smaller amount of positive charge is required to effectively bind the negative charge associated with the DNA. This assay therefore provides an excellent comparative method for considering the DNA affinities of a family of compounds such as this, in which each member has the same amine-derived DNA binding motif and, as such, is ideally suited for the development of structure—activity relationships. For this study, we compared all of our DNA binders under physiologically relevant salt concentrations (150 mM NaCl).

As indicated in Table 3, compounds **Z-G2** and **C_{12}-G2** were unable to effectively displace ethidium bromide from the DNA double helix under the conditions investigated. These compounds are the less effective dendrons in terms of self-assembly and should therefore not have such effectively organized multivalent arrays of DNA binding ligands. Each individual dendron only has a net positive charge of 8+, clearly insufficient to displace more than 50% of EthBr from its intercalation sites. Those dendrons which self-assemble more effectively, however, did achieve EthBr displacement, and CE_{50} values could be determined. As anticipated, **C_{22}-G2** was a more effective DNA binder than **C_{16}-G2**, presumably because of its greater self-assembly

Table 4. Selected Zeta Sizing Data for Short Strand DNA in the Presence of Dendrons

compound	N:P ratio	zeta (mV)	diameter (nm)[a:]
DNA	-----	−49.8 ± 1.8	---------
Z-G2	5	+6.2 ± 0.3	548.1 ± 25.2
C_{12}-G2	5	+5.85 ± 0.1	507.2 ± 59.4
C_{16}-G2	5	+18.5 ± 0.3	297.2 ± 16.1
C_{22}-G2	5	+45.5 ± 1.4	219.1 ± 1.21
Chol-G2	5	+48.8 ± 1.1	106.6 ± 0.4
$Chol_2$G2	5	+45.0 ± 1.0	79.7 ± 1.2

[a:] Average diameter assessed by Z-average in DLS measurements.

potential. The most effective DNA binders, however, were those with cholesterol groups at their focal points, with **$Chol_2$-G2** being slightly more effective than **Chol-G2**. Pleasingly, the experimentally verified CE_{50} values directly correlate with the surface charge density, σ_m, values estimated from simulation, indicating that the micelles characterized by higher values of σ_m (i.e., **$Chol_2$-G2**, **Chol-G2**, and **C_{22}-G2**) are tighter DNA binders than their counterparts with lower σ_m values (see Table 2).

The plasmid DNA binding affinity of the dendrons was then studied using gel electrophoresis with increasing amounts of dendron added to 1 μg of plasmid DNA. We used the dendron:DNA weight ratio necessary to fully retard the DNA in the loading well as an effective indicator of the DNA binding affinity of the vector. Table 3 reports the N:P ratio at which the DNA is fully retarded in the well (equivalent to a charge excess, CE, value). From the data, we can see that the cholesterol-functionalized dendrons were able to bind DNA at the lowest N:P ratio indicative of the most effective binding. Once again, for the aliphatic chain functionalized dendrons there was a correlation between aliphatic chain length and binding strength, with the shortest chain compound **C_{12}-G2** binding DNA with the lowest affinity and **C_{22}-G2** binding DNA much more effectively. Dendron **Z-G2**, which has no ability to self-assemble under the experimental conditions, binds to DNA with the lowest affinity of all the dendrons. It therefore appears that those compounds most effective at self-assembly are the strongest binders. It should be noted that the N:P values from gel electrophoresis are consistently higher than the CE_{50} values from the EthBr assay—this is because in electrophoresis we are looking for complete binding of plasmid, whereas in the EthBr assay, we are only looking for 50% displacement of the fluorescent dye. Gel electrophoresis images can be found in the Supporting Information.

We then carried out zeta sizing experiments of the complexes formed between the different dendrons and short strand DNA (see Supporting Information for full details). This allowed us to gain insight into the sizes of the complexes formed in the binding process and, as a consequence, the ability of the dendrons to condense plasmid DNA—an important step in the transfection pathway. Table 4 summarizes some of the key data which indicate that those dendrons which exhibit the highest affinity DNA binding as revealed by EthBr displacement and gel electrophoresis (i.e., **Chol-G2**, **$Chol_2$-G2**, and **C_{22}-G2**) are also those which condense the plasmid DNA most effectively into complexes which are typically ca. 100 nm in diameter (for full data see Supporting Information). The less effective DNA binders form aggregates with DNA which are ca. 500 nm in size—indicative of ineffective plasmid condensation and far too large for effective transfection. Furthermore, the dendrons which are better able to self-assemble form complexes with DNA which have a higher net positive charge, indicative of their better ability to neutralize the net anionic charge of the DNA.

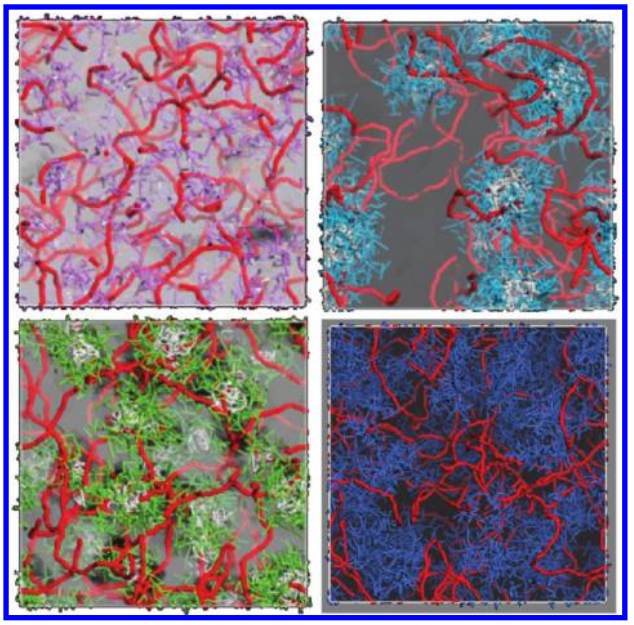

Figure 4. Mesoscale modeling of the hydrophobically modified dendrons synthesized in this work in the presence of DNA: **Z-G2** (top left); **Chol-G2** (top right); **C_{22}-G2** (bottom left), PEI (bottom right). In all pictures, white sticks represent hydrophobic units. Different colored sticks (purple, light blue, and green) are adopted to represent the various hydrophilic regions. DNA chains are depicted as red sticks. A transparent gray field is used to represent water.

We then carried out a mesoscale modeling study of the interactions between DNA and the dendron micelles. Conversion of the atomistic level structures into coarse-grained form and mapping the energetic information onto the appropriate value of the DPD interaction parameters a_{ij} allowed the mesoscale optimization of the interaction between self-assembled dendrons and extended DNA chains. The morphology of the self-assembled micelles and DNA helices is visualized in Figure 4 (see also Figure S8.4). As can be seen, the DNA molecules are loosely packed without a well-defined interhelical pattern or distances. The micelles appear to undergo a small degree of deformation in the complexes, with a tendency to elongate along the DNA longitudinal direction presumably to enhance the adhesion with the rather planar, extended surface of DNA (e.g., see **Chol-G2** in Figure 4). In these cases, the DNA molecules seem to comply with the well-known "bead-on-a-string" model,[32] according to which some regions of the nucleic acid are engulfed by the micelles while some others are no longer surrounded by them. Thus, the DNA helices are partially embedded within the micellar organization and partially exposed to the solution environment, where the counterions originating from the electrolyte provide the charge neutralization required for eventual condensation. Figure 4 (d) shows the results obtained from the mesoscopic simulations performed on the PEI/DNA system. These mesoscale results offer a sensible explanation for the high transfection capacity of PEI—the DNA is homogeneously intertwined between the PEI chains, so that it is quite efficiently protected from the outer environment. At the same time, since no particular structuring (e.g., beads on a necklace) is attained in solution, there are some areas where DNA bundles

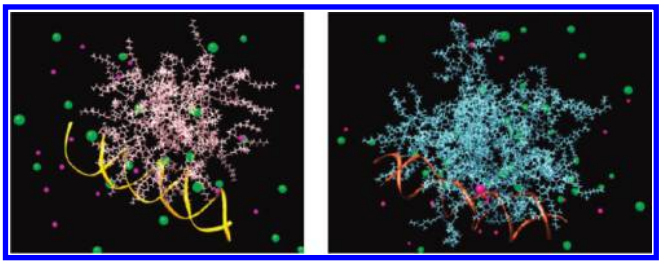

Figure 5. Atomistic MD simulations of a **Chol-G2** (pink, left) and a **Chol$_2$-G2** (light blue, right) micelle in complex with DNA (gold and orange ribbons). Na^+ and Cl^- ions are depicted as magenta and green spheres, respectively. Water is not shown for clarity.

Table 5. Binding Affinities between DNA and the Self-Assembled Dendron Micelles from Atomistic Level Modeling

Compound	ΔG_{bind} [a]	$\Delta G_{bind}/N$ [b]
C$_{12}$-G2	−16.8 ± 1.3	−0.35 ± 0.03
C$_{16}$-G2	−22.4 ± 1.7	−0.40 ± 0.03
C$_{22}$-G2	−33.8 ± 2.8	−0.47 ± 0.04
Chol-G2	−71.2 ± 3.1	−0.56 ± 0.02
Chol$_2$-G2	−119.2 ± 3.1	−0.68 ± 0.02
PEI	−269.0 ± 2.6	−0.63 ± 0.01

[a] ΔG_{bind} represents the free energy of binding between micelles and DNA in kcal mol^{-1}. [b] $\Delta G_{bind}/N$ is the normalized free energy per charge on the micelle.

appear and some free space which, ultimately, might yield better performance during release of this system.

The average number of DNA base pairs covered by each dendron micelle can be estimated to a first approximation by using the following, simple relationship: $n_{bp} = (D_m/3.4) \times 10$, where D_m is the spherical micelle diameter, 3.4 is the DNA duplex pitch (in nm), and 10 is the number of base pairs per duplex pitch. Inserting the estimated values of D_m listed in Table 2 in the above formula, we get n_{bp} = 15, 11.5, 9.7, 9.1, and 8.5 for **Chol$_2$-G2**, **Chol-G2**, **C$_{22}$-G2**, **C$_{16}$-G2**, and **C$_{12}$-G2**, respectively—in agreement with the observed DNA binding affinities (Table 3). The corresponding DNA phosphate groups per micelle are, however, not all bound directly to the micelle, considering the mismatch between the surface curvature of DNA and that of the micelle, even though, as discussed above, the dendritic micelles may elongate slightly along the DNA chain axis to maximize the favorable electrostatic interactions.

Quantitative modeling of micelle/DNA interactions at a fully atomistic level was used to rank the affinity of each type of modified dendron micelle toward DNA, ΔG_{bind}. Interactions between the ligands on the dendron and the grooves on the DNA double helix were clearly visible (Figure 5). As shown in Table 5, the MD-based MM/PBSA calculations indicated that **Chol$_2$-G2** is by far the most effective DNA binder, followed by **Chol-G2**, **C$_{22}$-G2**, **C$_{16}$-G2**, and **C$_{12}$-G2**, in agreement with the corresponding experimental evidence (Table 3). By considering the per charge normalized values of ΔG_{bind} on the micelle ($\Delta G_{bind}/N$), it is clear that **Chol$_2$-G2** is better able to utilize each charge in binding to the DNA double helix than **Chol-G2** and all other self-assembled systems. Focusing on the two tighter DNA binders, this observation, that **Chol$_2$-G2** binds DNA more strongly than **Chol-G2**, is consistent with, although somewhat larger in magnitude

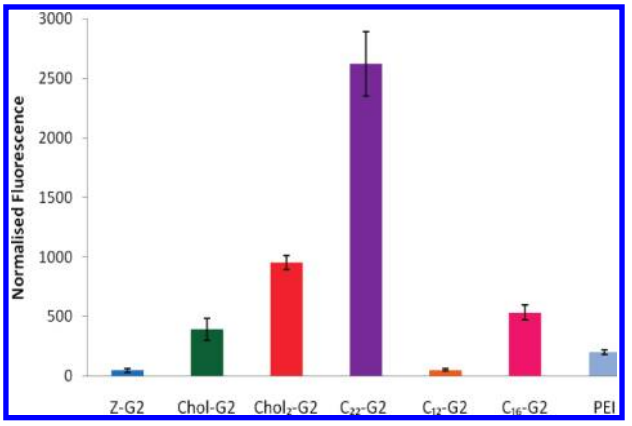

Figure 6. Fluorescence data for the uptake of fluorescently tagged DNA into HEK293 cells demonstrating effective cellular uptake by vectors **Chol-G2**, **Chol$_2$-G2**, **C$_{16}$-G2**, and **C$_{22}$-G2** which are best able to self-assemble into micellar aggregates. The data are corrected by subtraction of the uptake observed for plasmid DNA in the absence of any vector.

than, the experimental observations (Table 3). This is perhaps surprising given that modeling indicated that the **Chol$_2$-G2** self-assembled structures had lower surface charge densities than those resulting from **Chol-G2** (Table 2) and suggests that the larger micelle size of **Chol$_2$-G2** (Table 2) may play an important role in modulating the ability of the charges to bind to the DNA double helix without overcrowding at the micellar surface. Since PEI is a current standard vector system for DNA cell trasfection experiments, MD atomistic simulations were also run on a PEI/DNA for comparison. Interestingly, the estimated binding affinity of PEI toward DNA is, in terms of $\Delta G_{bind}/N$, somewhat intermediate between **Chol-G2** and **Chol$_2$-G2**. This finding is indicative of the fact that both cholesterol bearing, self-assembling dendrons possess excellent DNA binding properties which could be potentially exploited with success in gene delivery processes.

Gene Delivery into Cells. The ability of the dendron−DNA complexes to cross cell membranes was then investigated using flow cytometry. Human embryonic kidney cells (HEK293) were incubated with the vector mixed with fluorescently tagged plasmid DNA for 2 h at 37 °C. The cell uptake was measured using flow cytometry, and the fluorescence of any cells with characteristic dimensions for live cells was then recorded. The fluorescence is normalized to the value obtained for uptake of DNA alone, and the results are shown in Figure 6.

From the data, it can be clearly seen that the most hydrophobic dendrons, **Chol-G2**, **Chol$_2$-G2**, **C$_{16}$-G2**, and **C$_{22}$-G2**, demonstrated in the previous section to be capable of effective self-assembly and DNA binding are all capable of carrying DNA across cell membranes. Interestingly, they all do so even more effectively than positive control PEI. Indeed, compound **C$_{22}$-G2** is ca. 12 times more effective than PEI at getting DNA into live cells. To check that these results did not simply reflect the polyplexes sticking to cell surfaces, this experiment was repeated at 4 °C, and cell uptake was depressed to <20% of the levels observed at 37 °C for the two most effective delivery vehicles, **C$_{22}$-G2** and **Chol$_2$-G2** (see Supporting Information). In agreement with the self-assembly and DNA binding studies, **Z-G2** and **C$_{12}$-G2** show relatively poor cellular uptake, with activities only ca. 25% of that of PEI. The results of this study clearly indicate that cellular delivery can be directly correlated with the ability of

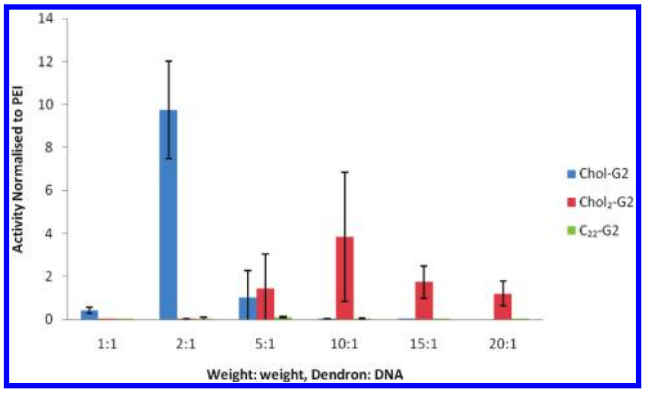

Figure 7. Transfection data for dendritic vectors in HEK 293 cells. Luciferase expression was normalized by total cellular protein; i.e., data were calculated in RLU/mg of protein and are then quoted as percentages of the transfection efficiency of PEI (N = 6, error bars represent standard deviation).

the dendrons to self-assemble, with hydrophobically modified dendrons showing a significant improvement on PEI. This demonstrates that these dendrons are well able to navigate barriers 1 and 2 to gene delivery (Figure 1). These flow cytometry results were also supported by confocal microscopy (see SI) which indicated cellular uptake of green-fluorescence tagged DNA after incubation for 1 h. The fluorescence associated with the DNA was spread within the cell and did not indicate localization in any specific organelle.

We then went on to investigate the ability of these dendrons to transfect cells. This experiment measures the ability of the dendrons to navigate all of the first five barriers on the pathway to gene delivery (as shown in Figure 1). The ability of the ester dendrons to transfect cells was studied using a luciferase expression assay. HEK293 cells were incubated for 4 h in serum-free media with mixtures of each dendron and plasmid (pGL3) DNA at different weight ratios. The transfection was then measured via luminescence assay after a further 20 h incubation in the presence of serum containing media. The transfection activity of the most effective dendrons as a percentage of the activity of polyethyleneimine (25k, branched) as a positive control[33] is shown in Figure 7. From the transfection data, we can see that **Chol-G2** was the most effective vector, with an activity of around 10% of that of PEI. **Chol$_2$-G2** showed some transfection at ca. 4% PEI positive control. **C$_{22}$-G2** only showed negligible levels, while **Z-G2**, **C$_{12}$-G2**, and **C$_{16}$-G2** exhibited no measurable transfection (data not shown in the figure).

Interestingly enough, the value of one of the micellar key parameters, the surface charge density σ_m, as estimated by our modeling procedures, correlates directly with the cellular transfection efficiency (TE) data discussed above. Indeed, the higher the value of σ_m, the higher the transfection efficiency of the corresponding system. This finding is not only qualitatively but also quantitatively in agreement with what is observed for cationic lipid/DNA-mediated delivery systems for which—depending on the morphological structure of the overall assembly—high values of σ_m are beneficial for achieving high TEs. Overall, however, none of the new dendrons perform as well as PEI, and this indicates that somewhere in steps 3−5 on the transfection pathway one of the barriers must be preventing overall transfection activity.

To consider barrier 3, endosomal escape, in more detail, we performed transfection in the presence of chloroquine. Previously,

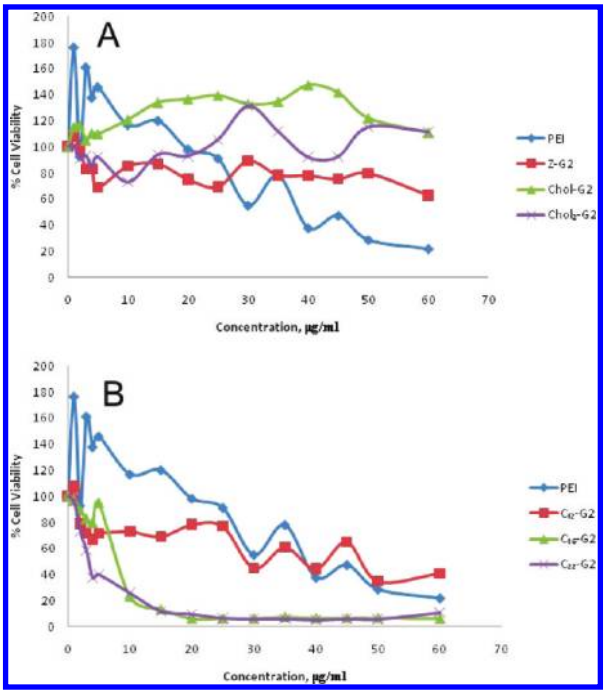

Figure 8. Percentage cell viability of HEK293 cells in the presence of: (A) **Z-G2**, **Chol-G2**, and **Chol$_2$-G2** and (B) **C$_{12}$-G2**, **C$_{16}$-G2**, and **C$_{22}$-G2**, at a range of different concentrations compared to that of 25 kDa PEI. Lines are drawn to guide the eye.

this basic drug has been used to enhance transfection levels by facilitating the endosomal escape process.[34] The transfection studies described above were therefore repeated in the presence of three different concentrations of chloroquine, 20, 50, and 100 μM. No enhancement in transfection levels was observed in any case, and this leads us to conclude that endosomal escape (barrier 3) is unlikely to be the rate-limiting step in gene delivery for these vectors. This is supported by the fact that no accumulation/localization of fluorescence within endosomes/lysosomes was detected by confocal microscopy (see SI). As such, we can conclude that barriers 4 and 5 are likely to be preventing effective gene transfection in this case.

We were concerned that one reason for ineffective gene transfection might be associated with vector toxicity, with the cells dying during the 24 h period of the assay. We therefore monitored toxicity using a commercial Cell Titer 96 assay (Promega). HEK293 cells were treated with the dendrons in serum free media and incubated for 4 h. Then the media was replaced with serum containing media, and the cells were incubated for a further 20 h.

The cholesterol-functionalized dendrons, **Chol-G2** and **Chol$_2$-G2**, are on their own completely nontoxic at the full range of concentrations measured (up to 60 μg/mL) (Figure 8A). Dendron **Z-G2**, on the other hand, has a toxicity similar to the PEI control, which is regarded as too toxic for clinical use.[13] The hydrocarbon chain-functionalized dendrons, however, showed very high toxicity. Indeed, the compounds with longer aliphatic chains, **C$_{16}$-G2** and **C$_{22}$-G2**, were significantly more toxic than 25 kDa PEI (Figure 8B). For this reason, although **C$_{22}$-G2** appeared optimum in terms of flow cytometry for its ability to cross cell membranes, it is clearly not appropriate for use in gene delivery. It is unclear why changing the hydrophobic group from a cholesterol moiety to a hydrocarbon chain has such a dramatic effect on the toxicity of these compounds, but it is possible that

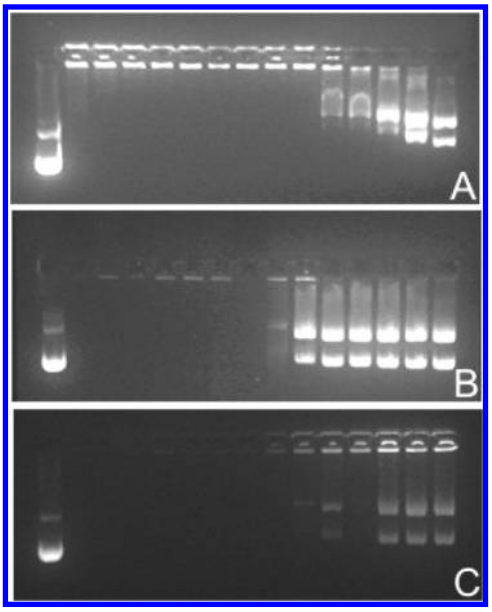

Figure 9. Gel electrophoresis images of pGL3 plasmid DNA (left-hand lane). The remaining lanes are dendron-bound plasmid DNA (5:1 wt/wt ratio) in the presence of increasing quantities of heparin sulfate (left to right)—lanes 2−15 (0:1 (heparin:DNA), 1:1, 2:1, 3:1, 4:1, 5:1, 7.5:1, 10:1, 15:1, 20:1, 25:1, 20:1, 35:1, 40:1). Image A, dendron = **Z-G2**; B, **Chol-G2**; C, **Chol$_2$-G2**.

the more flexible C_{22} hydrophobic unit is able to insert itself directly into cell membranes, disrupting normal cell behavior. In the presence of DNA, **Chol-G2** also showed significant levels of toxicity (50% cell viability at ca. 20 μg/mL). This may be a consequence of the good cellular uptake shown by this polyplex, followed by an inability to disassemble intracellularly (see below). Interestingly, **Chol$_2$-G2** showed lower toxicity when complexed to DNA.

DNA Release Studies. Given the conclusions from the gene delivery studies described above, we reasoned that although our dendrons self-assemble into highly effective multivalent DNA binders perhaps this binding is in fact too strong to facilitate intracellular DNA release. The ability of the dendrons to effectively release DNA was therefore investigated using a heparin sulfate displacement assay. Heparin sulfate is an anionic polymer, which can compete with DNA for binding to the cationic dendrons. The assay was performed via gel electrophoresis, using a fixed weight ratio of 5:1 vector:DNA in the wells and with increasing amounts of heparin sulfate being added to subsequent wells. The amount of heparin sulfate required to fully displace the DNA from the vector is a good indicator of how effectively the vector can release the DNA from its complex intracellularly.

Of all the vectors, it was interesting to note that **Chol-G2** shows the most effective DNA release (Figure 9), even though it is also one of the more effective DNA binders under these conditions. This dendron achieves full DNA release at a ratio of 20:1 (heparin:DNA), although very little DNA is released at lower weight ratios. This result correlates well with the transfection, where **Chol-G2** was found to be the most effective gene delivery agent. Dendrons **Z-G2** and **C$_{12}$-G2** (data not shown for **C$_{12}$-G2**) were the next most effective in terms of DNA release, with ratios of 35:1 heparin sulfate:dendron required for complete release. In the case of the remaining dendrons, **C$_{16}$-G2**, **C$_{22}$-G2** (data not shown), and **Chol$_2$-G2**, there was still incomplete release even at

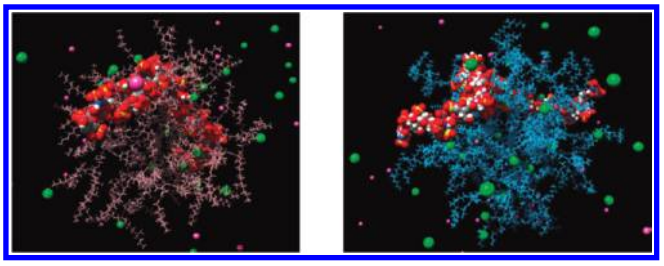

Figure 10. Atomistic MD simulations of a **Chol-G2** (pink, left) and a **Chol$_2$-G2** (light blue, right) in complex with heparin sulfate (atom-colored CPK spheres: red, O; blue, N; gray, C; white, H). Na^+ and Cl^- ions are depicted as magenta and green spheres, respectively. Water is not shown for clarity.

Table 6. Atomistic MD Modeling of the Binding to Heparin Sulfate of the Self-Assembled Dendron Micelles

	ΔG_{bind} [a]	$\Delta\Delta G_{bind}$ [b]
C$_{12}$-G2	−12.0 ± 0.7	4.8 ± 1.5
C$_{16}$-G2	−12.2 ± 1.1	10.2 ± 2.0
C$_{22}$-G2	−22.4 ± 1.9	11.4 ± 3.4
Chol-G2	−67.6 ± 1.5	3.6 ± 2.8
Chol$_2$-G2	−103.9 ± 2.6	15.3 ± 4.0

[a] ΔG_{bind} represents the free energy of binding between micelles and DNA in kcal mol^{-1}. [b] $\Delta\Delta G_{bind} = \Delta G_{bind}$(Heparin sulfate) − ΔG_{bind}(DNA) (see text for more details).

ratios of up to 40:1. This suggests that, particularly for **Chol$_2$-G2** which showed excellent DNA binding profiles and cellular uptake ability, ineffective DNA release (barrier 5 in the transfection pathway, Figure 2) is likely to be the cause of the low transfection levels observed. It is interesting to speculate that **Chol$_2$-G2** achieves more effective DNA binding as indicated both experimentally and by modeling methods, at the expense of effective DNA release, as the complex simply becomes too highly optimized and cannot be broken apart. **Chol-G2**, on the other hand, forms smaller micelles and slightly weaker complexes with DNA, facilitating intracellular DNA release. We noted that in this experiment PEI could be relatively easily displaced from the DNA by the addition of heparin (data not shown, ca. 15:1 heparin:DNA). This may agree with the morphology of the PEI/DNA aggregates as shown in Figure 4, in which there are some areas where DNA bundles appear between the PEI polymer chains and some free space which should cooperate in a better ability to release DNA from the overall complex.

The experimental heparin sulfate competition assays were paralleled by atomistic molecular dynamics simulation (Figure 10) of direct binding ΔG_{bind} of each dendron micelle and a chain of heparin sulfate. As shown in Table 6, MM/PBSA ranked **Chol$_2$-G2** as having the highest affinity toward heparin sulfate, followed by **Chol-G2**, **C$_{22}$-G2**, **C$_{16}$-G2**, and **C$_{12}$-G2**, respectively, in agreement with the affinities exhibited by these self-assemblies for DNA.

More enlightening information is however obtained by considering the last column in Table 6, presenting the difference in binding affinity of each dendron micelle toward heparin sulfate and DNA, respectively. Since here $\Delta\Delta G_{bind}$ is defined as $\Delta\Delta G_{bind} = \Delta G_{bind}$(heparin sulfate) − ΔG_{bind}(DNA), the more positive the value of $\Delta\Delta G_{bind}$ for a given dendron micelle, the higher the affinity of that micelle toward DNA rather than to

heparin sulfate. The data indicate that compound **Chol$_2$-G2** binds DNA much more effectively than heparin, while for **Chol-G2** the binding of heparin is much more competitive with DNA binding. This modeling study therefore verifies the experimental results provided by gel electrophoresis, in which **Chol-G2** was best able to release the DNA and transfection studies in which **Chol-G2** was the most effective delivery vehicle. This provides further support to the concept that, although beneficial for complexation, compaction, protection transport, and cellular entry, if DNA binding is too tight in comparison with other anionic species it is detrimental to the fundamental step of DNA release inside the target cell.

We propose that the better relative ability of **Chol-G2** to bind heparin and release DNA may be a consequence of the higher surface charge density of **Chol-G2** being better matched to the very high anionic surface charge density of heparin. We therefore reason that the cationic charge density of the self-assembled nanostructures may play an important role in enabling heparin-mediated DNA release. This would also explain why PEI, which has very high charge density, achieves such effective DNA release under these conditions.

Dendron Degradation and DNA Release. Our dendrons were designed to incorporate ester groups into the branched framework, providing them with the capacity to degrade under biological conditions of pH.[25] It had been our intention that over biologically relevant time scales dendron degradation would occur, turning a multivalent ligand array into smaller units which were not capable of such effective DNA binding.[6,7] We had hoped that this would actually facilitate intracellular DNA release, helping overcome barrier 5 to gene transfection, as well as breaking down the dendron into smaller nontoxic fragments (assisting with barrier 6 in the development of effective in vivo transfection agents). We therefore designed an electrospray mass spectrometric (ES-MS) assay to probe the pathways of dendron degradation which were actually taking place. A sample of each dendron was dissolved in aqueous buffer at pH 7.5 and stirred at 37 °C. Aliquots were removed from the bulk solution at regular time intervals and combined with dipeptide (glycine-alanine) at a fixed concentration as an internal standard. The samples were then analyzed by ES-MS, and the peak height of the molecular ion was monitored in relation to that of the standard. This allows the rate of degradation to be determined. It has been previously shown that similar dendrons fragment under ES conditions,[35] so the compound stability was set to 30% in the spectrometer to ensure that the peaks in the spectra were the result of degradation alone and did not correspond to spectrometer-induced fragmentation.

Figure 11 shows the mass spectra for **Chol-G2** taken at time zero and after 10 h stirring. In this way, and by considering the intermediate spectra, we could identify some of the products of degradation from the peaks which appear over time. Initially one of the ester bonds is cleaved, resulting in a carboxylic acid fragment and a larger alcohol-containing fragment of varying weight. After this initial ester hydrolysis, the carboxylic acid undergoes decarboxylation. Subsequently, the second branch becomes disconnected via ester hydrolysis. All of the dendrons effectively degrade via the same pathway (see Supporting Information).

By monitoring the ratio between the height of the molecular ion peaks and the peaks corresponding to the dipeptide, the rate of ester-hydrolysis-mediated degradation can be estimated. Plots of dendron concentration against time are shown in Figure 12. In all cases, the starting concentration of the dendron for the assay was 100 μM, and the concentration of the standard was constant

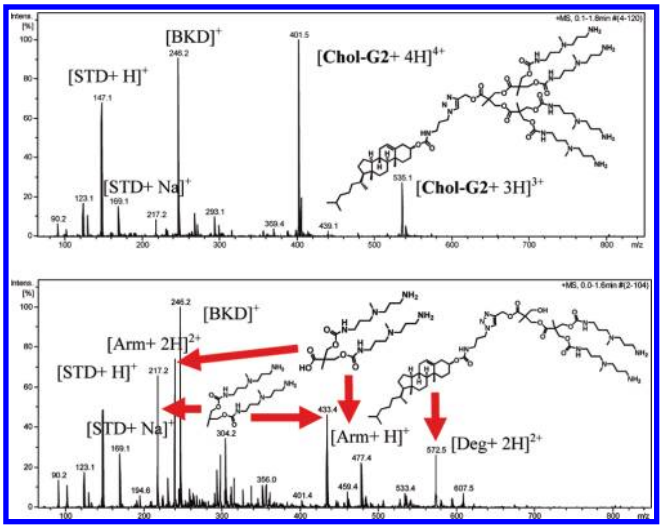

Figure 11. Electrospray mass spectrometry of **Chol-G2** from buffer at pH 7.4 at time zero (above) and after standing for 10 h (below). Degradation of the dendron framework can be clearly observed, as labeled.

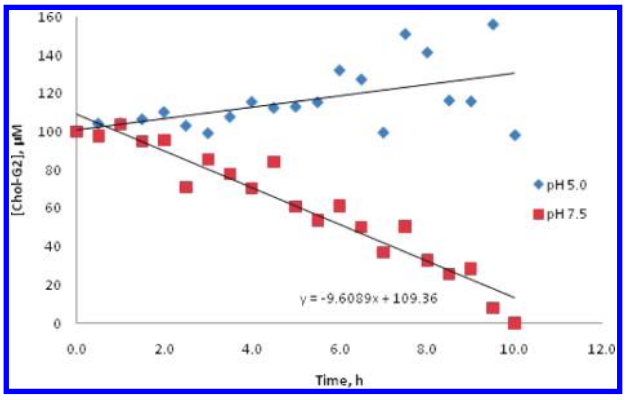

Figure 12. Time course of degradation for **Chol-G2** extracted from mass spectrometric data and determined at two different pH values (7.5 and 5.0), demonstrating that the dendron degrades at pH 7.5 but remains stable at pH 5.0.

at 500 μM. The degradation only monitors the loss of starting material and does not represent subsequent degradation steps. It exhibits zero-order kinetics with respect to dendron concentration as the concentration change is linear with respect to time. This demonstrates that there are no intermolecular interactions affecting the rate of degradation. We suggest it is possible that the amine groups on the dendron periphery may play an intramolecular role in catalyzing dendron degradation, which would explain why these dendrons degrade more rapidly under these conditions than those previously reported by Fréchet and coworkers.[25]

Data for all dendrons are tabulated in Table 7. As can be seen, dendron self-assembly does appear to have some effect on ester degradation. The non-self-assembling dendron **Z-G2** has an initial degradation rate of ca. 10.1 mmol dm^3 h^{-1}. The cholesterol functionalized dendrons have slightly lower rates of degradation, which might appear to indicate that self-assembly and effective packing of the cholesterol groups somewhat lower the degradation rate. However, for dendrons **C$_n$-G2** as the hydrophobic chain becomes

Table 7. Rates of Dendron Degradation in μmol dm^{-3} h^{-1}, Based on the Breakdown of the Initial Dendron, As Determined by the Mass Spectrometric Assay

dendron	rate of initial degradation/μmol dm^{-3} h^{-1}
Z-G2	10.1
C_{12}-G2	9.9
C_{16}-G2	12.2
C_{22}-G2	15.0
Chol-G2	9.6
$Chol_2$-G2	9.1

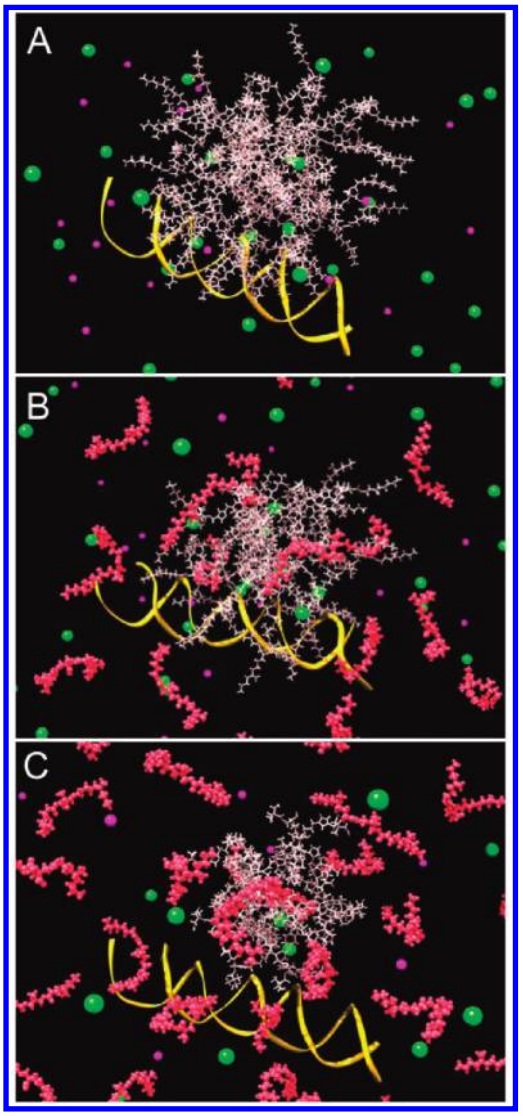

Figure 13. Images from the modeling of the degradation of **Chol-G2**. (A) represents intact **Chol-G2** binding DNA. (B) represents **Chol-G2** with half of the surface ligands detached. (C) represents **Chol-G2** with all of the surface ligands detached.

longer, the rate of degradation increases, which would indicate that in this case self-assembly appears to promote more effective degradation. Nonetheless, in general terms, all of the dendrons degrade, with none of the initial dendron (100 μM) remaining after a period of 6−10 h—a transfection relevant time scale.

Table 8. Atomistic Modeling of the Binding to DNA of the Self-Assembled Dendron Micelles with Sequential Ligand Detachment

dendron	number of ligands	ΔG_{bind}[a]	$\Delta G_{bind}/N$[b]
Chol-G2	4	−71.2 ± 2.4	−0.56 ± 0.02
	3	−47.7 ± 1.3	−0.50 ± 0.01
	2	−21.1 ± 1.1	−0.33 ± 0.02
	1	−10.0 ± 0.4	−0.31 ± 0.01
	0	−1.3 ± 0.1	
$Chol_2$-G2	4	−119.2 ± 3.1	−0.68 ± 0.02
	3	−82.6 ± 2.2	−0.63 ± 0.02
	2	−49.7 ± 1.6	−0.56 ± 0.02
	1	−14.0 ± 0.3	−0.32 ± 0.02
	0	−1.8 ± 0.1	

[a] ΔG_{bind} represents free energy of binding between micelles and DNA in kcal mol^{-1}. [b] $\Delta G_{bind}/N$ is the normalized free energy per charge on the micelle.

At first sight, therefore, the MS assay would indicate that dendron degradation should occur under cellular conditions and encourage DNA release. However, we also found that dendron degradation does not occur at pH 5.0, relevant to the interior of endosomes. It is known that ester hydrolysis in this type of dendron relies on base-catalyzed hydrolysis, and therefore, we argue that this degradation mode is switched off at pH 5.0.[25] We had thought that the carabamates may hydrolyze under this pH regime, in analogy to the results of Frechet and co-workers.[25] Clearly no carbamate hydrolysis takes place in our case. We assign the absence of carbamate hydrolysis either at pH 5.0 or pH 7.5 to the presence of protonated amines on the ligands proximal to the carbamate group, which would be expected to hinder the required protonation of the carbamate C═O group. It is therefore possible that during trafficking into the cell degradation of the dendron is limited as it experiences the more acidic endosomal environment and that this is responsible for the poor DNA release and transfection profile.

To confirm that dendron degradation should, in principle, lead to DNA release, we performed atomistic MD simulations. For this study, we detached surface ligands from the dendron by in silico degradation, and monitored the thermodynamics of binding by MM/PBSA calculations. The modeling is represented graphically in Figure 13, which illustrates how the micelle loses its ability to bind to DNA as surface ligands are detached in this manner. Table 8 collects the quantitative data which demonstrate that, as expected, the degraded products are less able to bind DNA than the intact dendrons when assembled into micellar form. Interestingly, the loss of DNA binding is more marked for **Chol-G2** than for **$Chol_2$-G2**. For **Chol-G2**, when half of the ligands have been lost (i.e., degradation of one of the ester bonds as evidenced by mass spectrometry), the binding strength for DNA has dropped by ca. 70%. However, for **$Chol_2$-G2**, loss of half the binding ligands only leads to a decrease in binding affinity of 58%. Only on further degradation does the free energy of DNA binding for **$Chol_2$-G2** drop significantly below 50 kcal mol^{-1}. We suggest that the two hydrophobic cholesterol units in **$Chol_2$-G2** are better able to maintain the self-assembled nanostructure during degradation, enabling the maintenance of a higher micellar surface positive charge density and allowing the micelles to hold onto DNA more effectively. These modeling observations would imply that if intracellular degradation is indeed occurring then

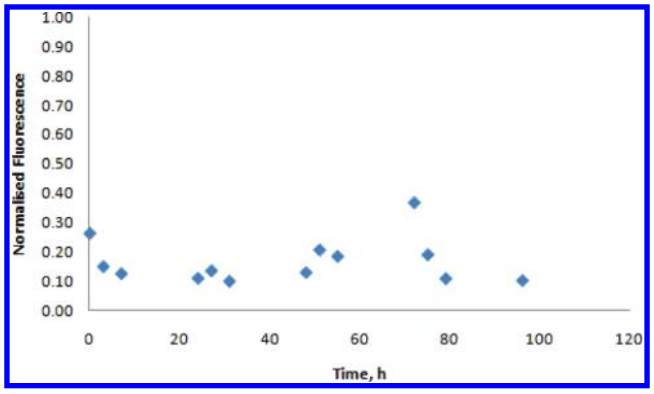

Figure 14. Fluorescence data demonstrating that on incubating a mixture of **Chol-G2**, calf thymus DNA, and ethidium bromide for extended periods of time the EthBr fluorescence remains quenched, indicating that the dendron does not release the DNA and allow reintercalation of the EthBr.

Chol-G2 would be the better dendron for achieving rapid DNA release, in agreement with our experimental observations of gene delivery.

To gain further insight into the process of DNA release and dendron degradation under biologically relevant conditions, we then designed an assay to monitor the DNA release capability of the self-assembling dendrons. This was achieved using a variant of the ethidium bromide (EthBr) assay in which calf thymus DNA, EthBr, and the DNA binder (either **Chol-G2** or **Chol$_2$-G2**) were mixed and incubated at 37 °C. This leads to a decrease in fluorescence as the EthBr is displaced from the DNA double helix by the presence of the dendron.

We reasoned that as the dendron degraded under these conditions it should release the DNA, and the EthBr would reintercalate into the DNA, switching its fluorescence back on. However, even on standing the solution for a period of 1 week, the EthBr fluorescence intensity remained essentially unchanged (Figure 14). This is in direct contrast to our previous studies, in which the dendron was degraded alone in buffer for a similar period of time and then shown to be completely incapable of binding DNA and displacing EthBr.[7] We therefore propose that complete degradation of the dendron *does not occur effectively when it is complexed to the DNA*. It is possible that the presence of the DNA prevents the base-catalyzed hydrolysis of ester bonds in a similar way to lowering pH or that once the amine groups are bound to the DNA they are no longer able to catalyze intramolecular breakdown of the dendron framework. As a consequence, we therefore propose that ineffective dendron degradation when bound to DNA is a primary cause of incomplete transfection and is a key problem associated with barrier 5 on the transfection pathway in this case.

CONCLUSIONS AND FUTURE WORK

We have reported a novel series of dendrons, in which it is demonstrated that self-assembly, DNA binding ability, and gene delivery potential can all be controlled in predictable ways by the nature of the functional group at the focal point. Multiscale modeling can be used to rationalize the DNA binding ability of all self-assembled nanostructures. Using a combination of experimental methods, it was then demonstrated that the dendrons could navigate barriers 1−4 on the transfection pathway. Pleasingly, it was noted that some of these vectors could significantly outperform PEI in terms of delivering DNA across cell membranes. However, we found that intracellular release of the DNA from the self-assembled vector was problematic.

The degradation of the dendrons was explored in detail, and it was found that although ester hydrolysis of one of the branches occurs on a transfection-relevant time scale (hours) this initial degraded system can still self-assemble and bind DNA quite effectively. Multilevel modeling was used to demonstrate that complete dendron degradation would be necessary for effective DNA release. Furthermore, when in the presence of lower pH associated with endosomes, or when bound to DNA, the degradation of these dendrons becomes ineffective on the transfection time scale—we propose that this explains the poor transfection performance of these dendrons.

As such, this integrated experimental and theoretical approach has provided a unique insight into the way in which gene delivery vectors can approach the multiple different extra- and intracellular barriers to gene delivery. Our primary target is now the development of high-affinity DNA binding systems with the potential to degrade, while still bound to DNA, under biologically useful time scales and at biologically relevant pH values. Clearly, future work on these vectors will therefore focus on enhancing the degradation pathways and enabling degradation-induced intracellular disassembly of the nanostructures. This kind of enhanced degradation process will trigger the loss of multivalency, improving DNA release, and ultimately enabling effective gene delivery.

ASSOCIATED CONTENT

Supporting Information. Full synthetic methods and characterization data for all new compounds, experimental methods for all DNA binding, gene delivery, toxicity and other assays, full details of mesoscale modeling methods, and additional data. This material is available free of charge via the Internet at http://pubs.acs.org.

AUTHOR INFORMATION

Corresponding Author
david.smith@york.ac.uk

ACKNOWLEDGMENT

We acknowledge The University of York and BBSRC for supporting this research through the award of a DTA studentship as well as the EU for assisting networking activities through the COST mechanism as part of TD0802 (Dendrimers in Biomedicine). Part of this work was carried out in the York Centre of Excellence in Mass Spectrometry, which was created thanks to a major capital investment through Science City York, supported by Yorkshire Forward with funds from the Northern Way Initiative. P.P. and S.P. wish to acknowledge the financial support from ESTECO through the project DDOS. D.W.P. acknowledges financial support from National Institutes of Health grants GM085222 and DK083875 (to M.E.H.).

REFERENCES

(1) (a) Rolland, O.; Turrin, C.-O.; Caminade, A.-M.; Marjoral, J.-P. *New J. Chem.* **2009**, 33, 1809–1824. (b) Boas, U.; Christensen, J. B.; Heegaard, P. M. H. *Dendrimers in Medicine and Biotechnology*; Royal Society of Chemistry: Cambridge, 2006. (c) Klajnert, B.; Bryszewska, M. *Dendrimers in Medicine*; Nova Science: UK, 2007. (d) Majoros, I. J.;

Baker, J. R. *Dendrimer-Based Nanomedicine*; Pan Stanford Publishing: Singapore, 2008.

(2) (a) Smith, D. K.; Hirst, A. R.; Love, C. S.; Hardy, J. G.; Brignell, S. V.; Huang, B. *Prog. Polym. Sci.* **2005**, *30*, 220–293. (b) Rosen, B. M.; Wilson, C. J.; Wilson, D. A.; Peterca, M.; Imam, M. R.; Percec, V. *Chem. Rev.* **2009**, *109*, 6275–6570.

(3) Posocco, P.; Pricl, S.; Jones, S. P.; Barnard, A.; Smith, D. K. *Chem. Sci.* **2010**, *1*, 393–404.

(4) (a) Mammen, M.; Choi, S. K.; Whitesides, G. M. *Angew. Chem., Int. Ed.* **1998**, *37*, 2754–2794. (b) Mulder, A.; Huskens, J.; Reinhoudt, D. N. *Org. Biomol. Chem.* **2004**, *2*, 3409–3424. (c) Badjic, J. D.; Nelson, A.; Cantrill, S. J.; Turnbull, W. B.; Stoddart, J. F. *Acc. Chem. Res.* **2005**, *38*, 723–732. (d) Huskens, J. *Curr. Opin. Chem. Biol.* **2006**, *10*, 537–543. (e) Martos, V.; Castreno, P.; Valero, J.; de Mendoza, J. *Curr. Opin. Chem. Biol.* **2008**, *12*, 698–706. (f) Welsh, D. J.; Smith, D. K. *Org. Biomol. Chem.* **2011**, *9*, 4795–4801.

(5) (a) Amir, R. J.; Pessah, N.; Shamis, M.; Shabat, D. *Angew. Chem., Int. Ed.* **2003**, *42*, 4494–4499. (b) Shamis, M.; Lode, H. N.; Shabat, D. *J. Am. Chem. Soc.* **2004**, *126*, 1726–1731. (c) Perry, R.; Amir, R. J.; Shabat, D. *New J. Chem.* **2007**, *31*, 1307–1312. (d) Sagi, A.; Segal, E.; Satchi-Fainaro, R.; Shabat, D. *Bioorg. Med. Chem.* **2007**, *15*, 3720–3727. (e) Sella, E.; Shabat, D. *Chem. Commun.* **2008**, 5701–5703. (f) Szalai, M. L.; Kevwitch, R. M.; McGrath, D. V. *J. Am. Chem. Soc.* **2003**, *125*, 15688–15689. (g) Kevwitch, R. M.; McGrath, D. V. *New J. Chem.* **2007**, *31*, 1332–1336. (h) de Groot, F. M. H.; Albrecht, C.; Koekkoek, R.; Beusker, P. H.; Scheeren, H. W. *Angew. Chem., Int. Ed.* **2003**, *42*, 4490–4494.

(6) (a) Kostiainen, M. A.; Smith, D. K.; Ikkala, O. *Angew. Chem., Int. Ed.* **2007**, *46*, 7600–7604. (b) Kostiainen, M. A.; Rosilo, H. *Chem.—Eur. J.* **2009**, *15*, 5656–5660. (c) Pavan, G. M.; Kostiainen, M. A.; Danani, A. *J. Phys. Chem. B* **2010**, *114*, 5686–5693. (d) Kostiainen, M. A.; Kotimaa, J.; Laukkanen, M. L.; Pavan, G. M. *Chem.—Eur. J.* **2010**, *16*, 6912–6918. (e) Kostiainen, M. A.; Kasyutich, O.; Cornelissen, J. J. L. M.; Nolte, R. J. M. *Nature Chem.* **2010**, *2*, 394–399.

(7) Welsh, D. J.; Jones, S. P.; Smith, D. K. *Angew. Chem., Int. Ed.* **2009**, *48*, 4047–4051.

(8) (a) Dufes, C.; Uchegbu, I. F.; Schatzlein, A. G. *Adv. Drug Delivery Rev.* **2005**, *57*, 2177–2202. (b) Guillot-Nieckowski, M.; Eisler, S.; Diederich, F. *New J. Chem.* **2007**, *31*, 1111–1127. (c) Smith, D. K. *Curr. Top. Med. Chem.* **2008**, *8*, 1187–1203.

(9) (a) Kukowska-Latallo, J.-F.; Bielinska, A. U.; Johnson, J.; Spindler, R.; Tomalia, D. A.; Baker, J. R. *Proc. Natl. Acad. Sci. U.S.A.* **1996**, *93*, 4897–4902. (b) Bielinska, A.; Kukowska-Latallo, J. F.; Johnson, J.; Tomalia, D. A.; Baker, J. R. *Nucleic Acids Res.* **1996**, *24*, 2176–2182.

(10) (a) Haensler, J.; Szoka, F. C. *Bioconjugate Chem.* **1993**, *4*, 372–379. (b) Tang, M. X.; Redemann, C. T.; Szoka, F. C. *Bioconjugate Chem.* **1996**, *7*, 703–714. (c) Turunen, M. P.; Hiltunen, M. O.; Ruponen, M.; Virkamaki, L.; Szoka, F. C.; Urtti, A.; Yla-Herttuala, S. *Gene Ther.* **1999**, *6*, 6–11.

(11) (a) Choi, J. S.; Lee, E. J.; Choi, Y. H.; Jeong, Y. J.; Park, J. S. *Bioconjugate Chem.* **1999**, *10*, 62–65. (b) Ohsaki, M.; Okuda, T.; Wada, A.; Hirayama, T.; Niidome, T.; Aoyagi, H. *Bioconjugate Chem.* **2002**, *13*, 510–517.

(12) (a) Wong, S. Y.; Pelet, J. M.; Putnam, D. *Prog. Polym. Sci.* **2007**, *32*, 799–837. (b) Tiera, M. J.; Winnik, F. M.; Fernandes, J. C. *Curr. Gene Ther.* **2006**, *6*, 59–71. (c) Midoux, P.; Breuzard, G.; Gomez, J. P.; Pichon, C. *Curr. Gene Ther.* **2008**, *8*, 335–352.

(13) (a) Lv, H.; Zhang, S.; Wang, B.; Cui, S.; Yan, J. *J. Controlled Release* **2006**, *114*, 100–109. (b) Duncan, R.; Izzo, L. *Adv. Drug Delivery Rev.* **2005**, *57*, 2215–2237.

(14) (a) Kuo, J.-h. S.; Lin, Y. L. *J. Biotechnol.* **2007**, *129*, 383–390. (b) Kuo, J.-h. S.; Liou, M.-j.; Chiu, H.-c. *Mol. Pharmaceutics* **2010**, *7*, 805–814.

(15) (a) Joester, D.; Losson, M.; Pugin, R.; Heinzelmann, H.; Walter, E.; Merkle, H. P.; Diederich, F. *Angew. Chem., Int. Ed.* **2003**, *42*, 1486–1490. (b) Guillot, M.; Eisler, S.; Weller, K.; Merkle, H. P.; Gallani, J. L.; Diederich, F. *Org. Biomol. Chem.* **2006**, *4*, 766–769. (c) Guillot-Nieckowski, M.; Joester, D.; Stohr, M.; Losson, M.; Adrian, M.; Wagner, B.; Kansy, M.; Heinzelmann, H.; Pugin, R.; Diederich, F.; Gallani, J. L. *Langmuir* **2007**, *23*, 737–746.

(16) (a) Toth, I.; Sakthivel, T.; Wilderspin, A. F.; Bayele, H.; O'Donnell, M.; Perry, D. J.; Pasi, K. J.; Lee, C. A.; Florence, A. T. *STP Pharm. Sci.* **1999**, *9*, 93–99. (b) Shah, D. S.; Sakthivel, T.; Toth, I.; Florence, A. T.; Wilderspin, A. F. *Int. J. Pharm.* **2000**, *208*, 41–48. (c) Al-Jamal, K. T.; Ramaswamy, C.; Singh, B.; Florence, A. T. *J. Drug Delivery Sci. Technol.* **2005**, *15*, 11–18. (d) Bayele, H. K.; Sakthivel, T.; O'Donell, M.; Pasi, K. J.; Wilderspin, A. F.; Lee, C. A.; Toth, I.; Florence, A. T. *J. Pharm. Sci.* **2005**, *94*, 446–457. (e) Bayele, H. K.; Ramaswamy, C.; Wilderspin, A. F.; Srai, K. S.; Toth, I.; Florence, A. T. *J. Pharm. Sci.* **2006**, *95*, 1227–1237.

(17) (a) Wood, K. C.; Little, S. R.; Langer, R.; Hammond, P. T. *Angew. Chem., Int. Ed.* **2005**, *44*, 6704–6708. (b) Wood, K. C.; Azarin, S. M.; Arap, W.; Pasqualini, R.; Langer, R.; Hammond, P. T. *Bioconjugate Chem.* **2008**, *19*, 403–405. (c) Poon, Z.; Lee, J. A.; Huang, S.; Prevost, R. J.; Hammond, P. T. *Nanomedicine* **2011**, *7*, 201–209.

(18) (a) Karmali, P. P.; Chaudhuri, A. *Med. Res. Rev.* **2007**, *27*, 696–722. (b) Bhattacharya, S.; Bajaj, A. *Chem. Commun.* **2009**, 4632–4656.

(19) (a) Kodama, K.; Katayama, Y.; Shoji, Y.; Nakashima, H. *Curr. Med. Chem.* **2006**, *13*, 2155–2161. (b) Mintzer, M. A.; Simanek, E. E. *Chem. Rev.* **2009**, *109*, 259–302.

(20) Edelstein, M. L.; Abedi, M. R.; Wixon, J. *J. Gene Med.* **2007**, *9*, 833–842.

(21) Kostiainen, M. A.; Hardy, J. G.; Smith, D. K. *Angew. Chem., Int. Ed.* **2005**, *44*, 2556–2559.

(22) (a) Hardy, J. G.; Kostiainen, M. A.; Smith, D. K.; Gabrielson, N. P.; Pack, D. W. *Bioconjugate Chem.* **2006**, *17*, 172–178. (b) Jones, S. P.; Gabrielson, N. P.; Pack, D. W.; Smith, D. K. *Chem. Commun.* **2008**, 4700–4702.

(23) Jones, S. P.; Gabrielson, N. P.; Wong, C.-H.; Chow, H.-F.; Pack, D. W.; Posocco, P.; Fermeglia, M.; Pricl, S.; Smith, D. K. *Mol. Pharm.* **2011**, *8*, 416–429.

(24) (a) Pavan, G. M.; Danani, A.; Pricl, S.; Smith, D. K. *J. Am. Chem. Soc.* **2009**, *131*, 9686–9694. (b) Jones, S. P.; Pavan, G. M.; Danani, A.; Pricl, S.; Smith, D. K. *Chem.—Eur. J.* **2010**, *16*, 4519–4532.

(25) (a) Ihre, H.; Hult, A.; Soederlind, E. *J. Am. Chem. Soc.* **1996**, *118*, 6388–6395. (b) Ihre, H.; Hult, A.; Fréchet, J. M. J.; Gitsov, I. *Macromolecules* **1998**, *31*, 4061–4068. (c) Ihre, H.; Padilla de Jesus, O. L.; Fréchet, J. M. J. *J. Am. Chem. Soc.* **2001**, *123*, 5908. (d) Gillies, E. R.; Fréchet, J. M. J. *J. Am. Chem. Soc.* **2002**, *124*, 14137–14146. (e) Gillies, E. R.; Dy, E.; Fréchet, J. M. J.; Szoka, F. C. *Mol. Pharmaceutics* **2005**, *2*, 129–138. (f) Lee, C. C.; Gillies, E. R.; Fox, M. E.; Guillaudeu, S. J.; Fréchet, J. M. J.; Dy, E. E.; Szoka, F. C. *Proc. Natl. Acad. Sci. U.S.A.* **2006**, *103*, 16649–16654.

(26) Wu, P.; Malkoch, M.; Hunt, J. N.; Vestberg, R.; Kaltgrad, E.; Finn, M. J.; Fokin, V. V.; Sharpless, K. B.; Hawker, C. J. *Chem. Commun.* **2005**, 5775–5777.

(27) Rodrigo, A. C.; Barnard, A.; Cooper, J.; Smith, D. K. *Angew. Chem., Int. Ed.* **2011**, *50*, 4675–4679.

(28) Stuart, M. C. A.; van de Pas, J. C.; Engberts, J. B. F. N. *J. Phys. Org. Chem.* **2005**, *18*, 929–934.

(29) (a) Hoogerbrugge, P. J.; Koelman, J. *Europhys. Lett.* **1992**, *19*, 155–160. (b) Español, P.; Warren, P. *Europhys. Lett.* **1995**, *30*, 191–196. (c) Groot, R. D.; Warren, P. B. *J. Chem. Phys.* **1997**, *107*, 4423–4435. (d) Groot, R. D.; Rabone, K. L. *Biophys. J.* **2001**, *81*, 725–736.

(30) (a) Israelachvili, J. N.; Mitchell, D. J.; Ninham, B. W. *J. Chem. Soc., Faraday Trans. 2* **1976**, *72*, 1525–1568. (b) Israelachvili, J. N.; Mitchell, D. J.; Ninham, B. W. *Biochim. Biophys. Acta* **1977**, *470*, 185–201.

(31) (a) Cain, B. F.; Baguley, B. C.; Denny, W. A. *J. Med. Chem.* **1978**, *21*, 658–668. (b) Gershon, H.; Ghirlando, R.; Guttman, S. B.; Minsky, A. *Biochemistry* **1993**, *32*, 7143–7151.

(32) (a) Wong, H.; Victor, J. M.; Mozziconacci, J. *PLos One* **2007**, *2* (9), e877. (b) Abdelhady, H. G.; Allen, S.; Davies, M. C.; Roberts, C. J.; Tendler, S. J. B.; Williams, P. M. *Nucleic Acid Res.* **2003**, *31*, 4001–4005. (c) Dorigo, B.; Schalch, T.; Kulangara, A.; Duda, S.; Schroeder, R.; Richmond, T. J. *Science* **2004**, *306*, 1571–1573. (d) Olins, A. L.; Olins, D. E. *Science* **1974**, *183*, 330–332.

(33) (a) Thomas, M.; Klibanov, A. M. *Proc. Natl. Acad. Sci. U.S.A.* **2002**, *99*, 14640–14645. (b) Forrest, M. L.; Koerber, J. T.; Pack, D. W. *Bioconjugate Chem.* **2003**, *14*, 934–940. (c) Gabrielson, N. P.; Pack, D. W. *Biomacromolecules* **2006**, *7*, 2427–2435. (d) Gabrielson, N. P.; Pack, D. W. *J. Controlled Release* **2009**, *136*, 54–61.

(34) (a) Guy, J.; Drabek, D.; Antoniou, M. *Mol. Biotechnol.* **1995**, *3*, 237–248. (b) Pless, D. D.; Wellner, R. B. *J. Cell. Biochem.* **1996**, *62*, 27–39. (c) Erbacher, P.; Roche, A. C.; Monsigny, M.; Midoux, P. *Exp. Cell Res.* **1996**, *225*, 186–194.

(35) Baytekin, B.; Baytekin, H. T.; Hahn, U.; Reckien, W.; Kirchner, B.; Schalley, C. A. *Chem.—Eur. J.* **2009**, *15*, 7139–7149.